Neurosci. Bull. February, 2019, 35(1):15–24
https://doi.org/10.1007/s12264-018-0271-1

www.neurosci.cn
www.springer.com/12264

ORIGINAL ARTICLE

Anti-Hypertensive Action of Fenofibrate *via* UCP2 Upregulation Mediated by PPAR Activation in Baroreflex Afferent Pathway

Jian Guan[1] · Miao Zhao[1] · Chao He[1] · Xue Li[1] · Ying Li[1] · Jie Sun[1] · Wei Wang[1] · Ya-Li Cui[1] · Qing Zhang[1] · Bai-Yan Li[1] · Guo-Fen Qiao[1]

Received: 5 January 2018 / Accepted: 29 May 2018 / Published online: 1 September 2018

Abstract Fenofibrate, an agonist for peroxisome proliferator-activated receptor alpha (PPAR-α), lowers blood pressure, but whether this action is mediated *via* baroreflex afferents has not been elucidated. In this study, the distribution of PPAR-α and PPAR-γ was assessed in the nodose ganglion (NG) and the nucleus of the solitary tract (NTS). Hypertension induced by drinking high fructose (HFD) was reduced, along with complete restoration of impaired baroreceptor sensitivity, by chronic treatment with fenofibrate. The molecular data also showed that both PPAR-α and PPAR-γ were dramatically up-regulated in the NG and NTS of the HFD group. Expression of the downstream signaling molecule of PPAR-α, the mitochondrial uncoupling protein 2 (UCP2), was up-regulated in the baroreflex afferent pathway under similar experimental conditions, along with amelioration of reduced superoxide dismutase activity and increased superoxide in HFD rats. These results suggest that chronic treatment with fenofibrate plays a crucial role in the neural control of blood pressure by improving baroreflex afferent function due at least partially to PPAR-mediated up-regulation of UCP2 expression and reduction of oxidative stress.

Keywords Fenofibrate · Peroxisome proliferator-activated receptor · Mitochondrial uncoupling protein · Baroreflex afferent function · Blood pressure regulation

Introduction

Peroxisome proliferator-activated receptor alpha (PPAR-α), a member of the nuclear receptor superfamily of ligand-activated transcription factors, is involved in almost all aspects of lipid metabolism, including the uptake, binding, and oxidation of fatty acids, lipoprotein assembly, and lipid transport [1, 2]. PPAR-α is expressed mainly in the liver, kidney, and skeletal muscle where it is involved in fatty acid oxidation. Furthermore, PPAR-α is expressed in cardiovascular cells where it has anti-inflammatory and antioxidant effects [3, 4]. PPAR-γ is widely expressed in adipose tissue, and is involved in metabolic dysregulation and cancer progression [5]. Fibrates are a class of compounds currently used in the treatment of obesity, hyperlipidemia, and type-2 diabetes, targeting PPAR-α [6–8]. Recent studies have demonstrated that induction of the fibroblast growth factor 21 gene by PPAR-α [9] downregulates blood pressure *via* baroreflex afferent function [10]. However, little is known about the effect and underlying mechanism of fenofibrate (an FDA-approved agonist for PPAR-α) on the neural control of blood pressure even though the following are thought to be linked to fenofibrate action: reduction of myocardial fibrosis and glomerular hypertrophy [11, 12], elevation of superoxide dismutase in adult mouse brain microvessels, and protective effects on the nervous and cardiovascular systems [13, 14].

With reference to hypertension, PPAR-α is closely associated with the regulation of blood pressure [15, 16].

Electronic supplementary material The online version of this article (https://doi.org/10.1007/s12264-018-0271-1) contains supplementary material, which is available to authorized users.

✉ Bai-Yan Li
liby@ems.hrbmu.edu.cn

✉ Guo-Fen Qiao
qiaogf88@163.com

[1] Department of Pharmacology (State-Province Key Laboratories of Biomedicine-Pharmaceutics of China, Key Laboratory of Cardiovascular Medicine Research, Ministry of Education), College of Pharmacy, Harbin Medical University, Harbin 150081, China

Likewise, fenofibrate reduces blood pressure and/or prevents the development of hypertension in animal models of insulin resistance and/or hypertension [17]. However, the involvement of fenofibrate-mediated PPAR-α activation in the amelioration of hypertension *via* the baroreflex afferent pathway has not been revealed. Notably, the baroreflex afferent pathway is composed of baroreceptor terminals at the aortic arch, the nodose ganglion (NG) and nucleus of the solitary tract (NTS), which sense and relay the signal of blood pressure change and play a pivotal role in the neural mechanism of hypertension [10, 18]. Impairment of baroreflex afferent function is closely associated with the hypertension linked to metabolic syndrome and obesity [19, 20], which complies well with the notion that changes in the expression of PPAR-α/PPAR-γ occur in the NTS and NG under hypertensive conditions [21, 22]. Thus, it is essential to confirm the role of fenofibrate in the neural control of blood pressure and its contribution to the metabolic syndrome-related pathogenesis of hypertension.

Oxidative stress, greater production than degradation of reactive oxygen species, is closely associated with hypertension [23–25]. The mitochondrial uncoupling protein-2 (UCP2) plays an important role in anti-oxidation, energy balance, and metabolic regulation [26, 27], and is itself regulated by PPAR-α and PPAR-γ [23]. Therefore, in this study, hypertension was induced in rats drinking high fructose as a metabolic syndrome-related hypertension model [28, 29] and we tested the hypothesis that chronic treatment with fenofibrate has a significant antihypertensive effect by up-regulation of UCP2 through the baroreflex afferent pathway after PPAR-α activation in high fructose-drinking (HFD) rats.

Materials and Methods

Animals

All animal protocols were approved by the Institutional Animal Care and Use Committee of Harbin Medical University, and were in accord with the recommendations of the Panel on Euthanasia of the American Veterinary Medical Association and the National Institutes of Health Guide for the Care and Use of Laboratory Animals (http://www.nap.edu/readingroom/books/labrats/). Male Sprague-Dawley rats weighing 200 g–250 g were purchased from the Experimental Animal Center of the Second Affiliated Hospital of Harbin Medical University (Harbin, China).

The key experimental procedures were the measurement of systolic blood pressure (SBP) in conscious rats using the tail-cuff method and short axis (SAX) recording by echocardiography, computation of baroreflex sensitivity (BRS), and the collection of NTS and NG tissues for molecular and immunohistochemical studies to assess the expression level of mRNA or protein.

Hypertension in Rats Induced by Drinking High-Fructose

All rats were fed normal laboratory rat chow and water. Rats were maintained on a 12-h light/dark cycle at 25°C and randomly divided into two experimental groups after one week of adaptation. Following a previous report [30], the rats in the control group (Ctrl) continued on a diet of chow and normal water, while the rats in the hypertension group induced by HFD drank water containing 10% (*w*/*v*) fructose (Zhiyuan Chemical Co., Binzhou, China) for 7 weeks. After 7 weeks, the HFD rats with an average SBP $\geq$ 135 mmHg were selected as the HFD models.

Chronic Fenofibrate Treatment Scheme

HFD and Ctrl rats were fed a diet containing fenofibrate (100 mg/kg per day) [31, 32] (Sigma, St. Louis, MO) for 4 weeks (HFD + FF-4w, and Ctrl + FF-4w). The HFD + FF-4w rats were regarded as HFD models with an averaged SBP $\geq$ 127 mmHg after 3 weeks of HFD and fed with fenofibrate for 4 weeks. All experimental protocols complied with the Guide for the Care and Use of Laboratory Animals.

Systolic Blood Pressure Measurements

The SBP of all rats was measured once a week with a manometer-tachometer (BP-2010E, Softeron Biotechnology, Beijing, China) using the tail-cuff method. Rats were restrained in a plastic holder in a quiet temperature-controlled (36°C) environment. The average SBP for each rat was obtained from five readings after it had adapted to the environment. The values from 8 rats in each group were averaged again as one data point.

Echocardiographic Measurements

Trans-thoracic echocardiography with an ultrasound machine (Vevo 2100 imaging system, VisualSonics, Toronto, Canada) was used to assess the heart functions of normal Ctrl, HFD, Ctrl + FF-4w, and HFD + FF-4w rats (n = 6/group). Left ventricular systolic/diastolic internal diameter (LVIDs/LVIDd, mm), interventricular septum systolic/diastolic thickness (IVSs/IVSd, mm), left ventricular systolic/diastolic anterior wall (LVAWs/LVAWd, mm), and left ventricular systolic/diastolic posterior wall (LVPWs/LVPWd, mm) were measured. Ejection fraction (EF, %) and fractional shortening (FS, %) were calculated from SAX or parasternal long axis-mode recording.

Baroreflex Sensitivity

Following the previous protocol [33, 34], one cannula was inserted into the femoral artery and another into the femoral vein of the anesthetized rat (3% amobarbital sodium, 25 mg/kg, i.p.). The cannula in the femoral artery was filled with heparin-saline. The arterial cannula (left) was used for arterial pressure measurement and the venous cannula (right) for drug administration. The electrocardiogram was recorded (LabChart 7 Pro software, AD instruments, Bella Vista, Australia) and body temperature was maintained at ~ 35°C. After postsurgical equilibration, sodium nitroprusside (SNP, Sigma, St. Louis, MO) and phenylephrine (PE, Sigma) at incremental doses (1.0, 3.0, and 10 μg/kg) were injected intravenously to induce acute decreases and increases in blood pressure, respectively. After each injection, the maximum change in heart rate at the peak change in mean arterial pressure (MAP) were recorded and Δheart rate/ΔMAP was calculated as an index of baroreceptor gain.

Tissue Preparation

The NG was dissected as we previously described [34, 35]. Briefly, unrestrained rats were placed in an airtight induction chamber for inhalation of the anesthetic Metofane (methoxyflurane, Schering-Plough Animal Health Corp, Kenilworth, NJ). Upon loss of the reflex response to tail pinch the animals were immediately opened at the mid-axillary region in order to preserve enough of the vagus nerve to easily find the NG toward its distal end. The entire NG with the attached nerve trunk was carefully excised under a stereo-microscope (40×, Olympus, Tokyo, Japan) and immediately transferred to a Petri dish containing chilled (4°C) normal saline. Then the surrounding connective tissue was gently removed and the NG was stored in liquid nitrogen until further investigation. The NTS was also carefully and quickly dissected from a 1-mm thick brainstem slice at the level of the obex under a microscope and with similar experimental conditions. Briefly, the rats were deeply anesthetized with ether and quickly killed by cervical dislocation. The hindbrain was removed as quickly as possible and placed for 1 min in freezing (−3°C to 0°C) artificial cerebrospinal fluid. The medulla was trimmed rostrally and caudally to yield a 1-cm block centered on the obex. After removing the cerebellum, the block was ready for experimental use or kept in liquid nitrogen for later investigation.

Quantitative Real-Time Polymerase Chain Reaction (qRT-PCR)

One mRNA sample of NG or NTS tissue was harvested from 4–5 rats in each group (Ctrl, Ctrl + FF-4w, HFD, and HFD + FF-4w). Following the manufacturer's instructions, the mRNA expression was determined using an ABI 7500 fast Real-Rime PCR System (Applied Biosystems, Foster City, CA). The primers (Invitrogen, Frederick, MD) used in this investigation are listed in Table S1. The data of relative mRNA expression were analyzed with the $2^{-\Delta\Delta Ct}$ method [36].

Immunoblotting Analysis

The NTS or NG was homogenized in isolation buffer. The total protein was extracted from 4–5 (NTS) or 6–8 (NG) rats in each group incubated for 1 h at 4°C in RIPA buffer containing 1% protease inhibitor. Briefly, proteins from the NTS (100 μg/sample) or from the NG (80 μg/sample) extracts were separated on 10% SDS-PAGE and transferred to nitrocellulose membranes, which were further blocked with 5% non-fat dry milk for 2 h, then incubated at 4°C overnight or for 18 h with the primary antibodies anti-GAPDH (internal control, Sigma), anti-PPAR-α (1:500, Sigma), anti-PPAR-γ (1:500, Sigma), and anti-UCP2 (1:500, Sigma). This was followed by incubation with the appropriate secondary antibodies (anti-rabbit/anti-goat) (1:8000; LI-COR Biosciences, Lincoln, NE) at room temperature for 50 min–60 min. Specific antibody-antigen complexes were detected using the Odyssey Infrared Imaging System (LI-COR Biosciences, Waltham, MA).

Immunohistochemistry and Visualization of Whole NTS Sections

The immunohistochemistry protocol for the NG was as described in our previous report [37]. As we previously described, for the visualization of whole sections in immunohistochemistry experiments, brainstem sections (35 μm thick, bregma –12.6 mm) were washed in phosphate-buffered saline (PBS) for 10 min before immunostaining, and blocked in 4% normal goat serum/0.3% Triton X-100/PBS for 1.5 h at 37°C. For double-labeling, sections were incubated with the primary antibodies anti-PPAR-α (1:200, Sigma) and anti-PPAR-γ (1:500, Sigma) in blocking solution overnight at 4°C. The sections were washed three times with phosphate buffer solution (PBST) for 10 min each, and then incubated with the secondary antibody mixture for anti-PPAR-α and anti-PPAR-γ, and anti-rabbit IRDye 680RD (LI-COR Bioscience) diluted to 1:5000 in PBS, at room temperature for ~1 h. The sections were washed five times in PBST for 10 min each. Finally, fluorescent immunocomplexes were measured using a LI-COR Odyssey infrared imaging system.

Superoxide Levels and Superoxide Dismutase Activity in the NTS

The level of the superoxide anion in isolated NTS tissues was measured using a superoxide assay kit (WST-1, S0060) and a superoxide dismutase activity kit (NBT, S0109) from Beyotime Institute of Biotechnology (Shanghai, China).

Statistical Analyses

Differences between two groups were analyzed using the two-tailed unpaired Student's *t*-test, while one- or two-way ANOVA followed by Bonferroni's *post hoc* test was used for more than two groups. $P < 0.05$ was considered statistically significant. Data are expressed as mean ± SD.

Results

Distribution of PPAR-α/γ by Immunostaining in the NG and NTS Regions

The NG and NTS house the 1st- and 2nd-order visceral afferent neurons, including baroreceptor and baroreceptive neurons, respectively, in the baroreflex afferent pathway. Therefore, exploring the distribution and expression profiles of both PPAR-α and PPAR-γ in the NG and NTS would be the first step to understand whether the PPAR activator fenofibrate exerts a significant anti-hypertensive effect *via* the manipulation of PPAR-α and PPAR-γ expression. To test this hypothesis, we investigated the distribution of PPAR-α and PPAR-γ in the NTS and NG using immunohistochemical detection with specific antibodies against PPAR-α or PPAR-γ. In this experiment, whole-section visualization showed that PPAR-α fluorescence was detected in both the cytoplasm and nucleus of NG neurons, while PPAR-γ fluorescence was only observed in the nucleus ($n = 6$ duplications, Fig. 1A), and dramatic PPAR-α fluorescence was also detected in the NTS region ($n = 6$ duplications; bregma −12.60 mm, Paxinos and Watson, 2007; Fig. 1B). Furthermore, the mRNA expression of PPAR-α and PPAR-γ was confirmed by qRT-PCR ($n = 6$ duplications, Fig. 1C) in the NTS and NG tissues with significantly higher expression of PPAR-α than PPAR-γ. These observations strongly suggest potential crucial roles of PPAR-α and PPAR-γ in the neural control of blood pressure *via* the afferent baroreflex pathway.

Neural Control of Blood Pressure by Chronic Treatment with Fenofibrate in HFD Rats

To further test the anti-hypertensive action of PPAR-α or PPAR-γ, we applied fenofibrate directly to activate PPAR-α in HFD-induced hypertensive (HFD-HTN) rats as an independent metabolic syndrome-related hypertension model. The SBP gradually and significantly increased in the HFD-HTN rats during the seven weeks of HFD compared to normal controls (Ctrl, $P < 0.01$, $n = 8$ rats/group; Fig. 2A). Based on this model, we investigated the cardiovascular effects of chronic fenofibrate by gavage in HFD rats for four consecutive weeks. The results showed that fenofibrate did not change the baseline SBP ($P > 0.05$) or MAP (Ctrl + FF-4w *vs* Ctrl, $P > 0.05$, $n = 8$ rats/group) during the four weeks of observation (Fig. 2A, B). However, compared with the HFD group, fenofibrate (100 mg/kg per day) for four weeks significantly decreased both SBP and MAP in conscious HFD rats (HFD + FF-4w *vs* HFD, $P < 0.05$ or < 0.01, $n = 8$ rats/group) without any detectable change in heart rate (Fig. 2C) in either control or HFD rats under the same experimental conditions.

BRS, the best representation of baroreflex afferent function, and molecular and immunostaining analysis all pointed to the potential involvement of PPAR activation in this pathway. Furthermore, BRS (ΔHR/ΔMAP, bpm/mmHg) was further investigated in anesthetized rats with the protocol reported previously [10]. Clearly, fenofibrate did not alter the baseline BRS at the concentrations of both PE (1 μg/kg, 3 μg/kg, or 10 μg/kg) and SNP (1 μg/kg, 3 μg/kg, or 10 μg/kg). Apparently, the change in BRS was aberrantly decreased in the HFD group by intravenous injections of PE and was significantly reversed by fenofibrate treatment for 4 weeks (HFD + FF-4w *vs* HFD: PE 1, 3, and 10, $P < 0.05$, $n = 6$ rats/group, Fig. 2D). However, this tendency did not appear after intravenous injection of SNP (Fig. 2E) under the same experimental conditions.

Consistently, the echocardiographic results showed that fenofibrate did not influence any of the parameter in control rats (Ctrl *vs* Ctrl + FF-4w, $P > 0.05$, $n = 6$ rats/group), while in HFD rats, the SAX M-mode indicated an enlarged LVIDd (7.57 ± 0.08 mm, $P < 0.05$) compared with the control, and this increased LVIDd was clearly restored to near the control level after 4 weeks of chronic fenofibrate treatment (6.98 ± 0.52 mm, $P < 0.05$ *vs* HFD rats; Fig. 3, Table 1).

Dysregulation of PPAR-α and PPAR-γ in the Baroreflex Afferent Pathway in HFD Rats

Our molecular and functional studies have demonstrated the clear distribution of PPARs in the baroreflex afferent pathway and robust reversal effects of fenofibrate in HFD-induced hypertension; this strongly suggests a role of the dysregulation of PPARs, the receptors for their ligand fenofibrate, in the current hypertensive model. In this regard, we further investigated the expression of PPAR-α and PPAR-γ at the tissue level of the NG and NTS in HFD rats. In the NG, the results from qRT-PCR showed significant mRNA upregulation of both PPAR-α and PPAR-γ in the

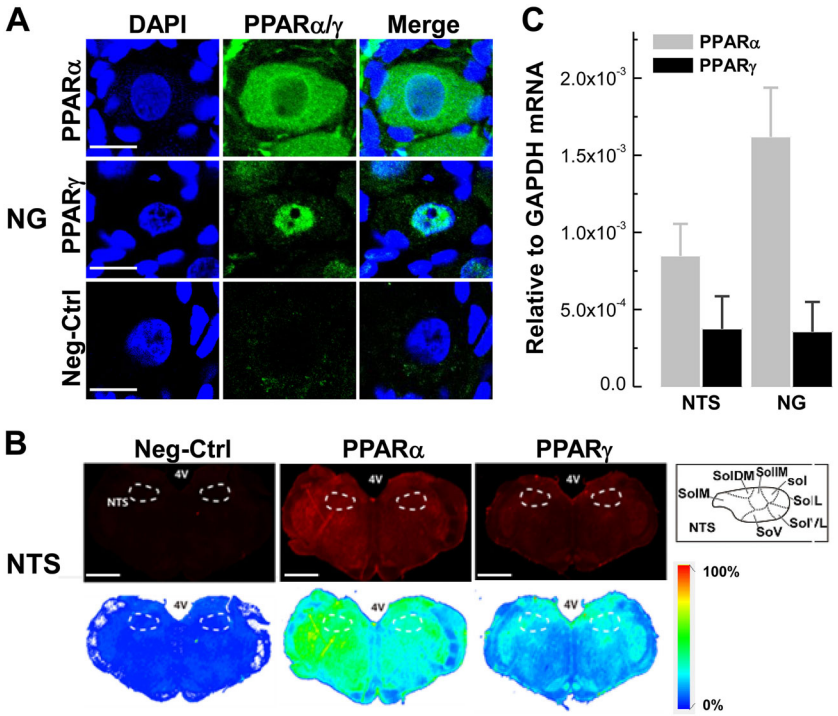

Fig. 1 Distribution of PPAR-α/PPAR-γ mRNA and protein on the NG and NTS. **A** Immunostaining of PPAR-α/PPAR-γ protein in NG tissue sections (7 μm). DAPI staining indicates nuclei (blue). Scale bars, 50 μm; $n = 6$ duplications. **B** Immunostaining of whole brainstem sections (35 μm; bregma, −12.60 mm) showing the distribution of PPAR-α/PPAR-γ protein in the NTS region. Scale bars, 2 mm; $n = 6$ duplications. **C** Levels of mRNA expression of PPAR-α/PPAR-γ in the NTS and NG of normal rats. $n = 6$ duplications. The condition with no primary antibody was set as the negative control. 4 V, 4th ventricle; Sol, solitary tract; SolL, lateral Sol; SolVL, ventrolateral Sol; SolV, ventral Sol; SolM, medial Sol; SolDM, dorsomedial Sol; SolIM, intermediate Sol.

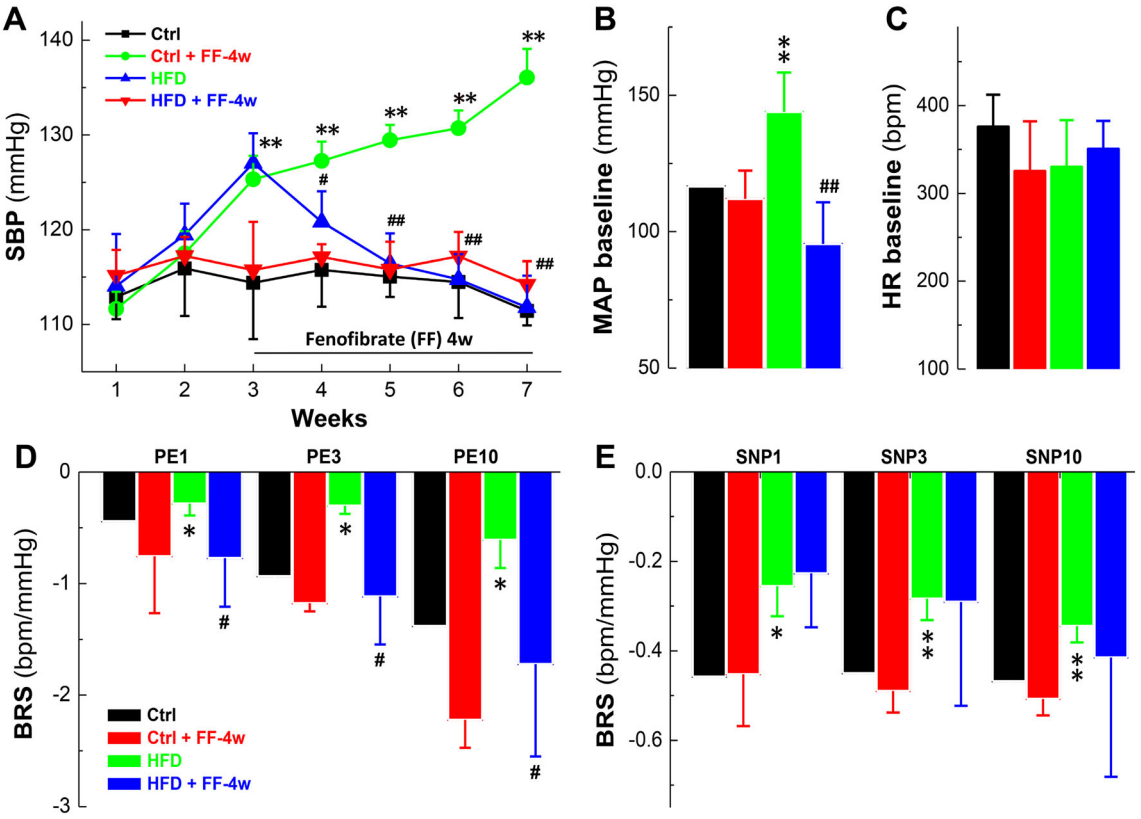

Fig. 2 Protective cardiovascular effects of chronic fenofibrate treatment in HFD rats. **A** SBP of control and HFD rats with fenofibrate treatment for 4 weeks (4w), $n = 8$ rats/group. **B–C** MAP (mmHg) and heart rate (HR) baselines. **D–E** BRS (bpm/mmHg) induced by PE or SNP-1/3/10 (phenylephrine or sodium nitroprusside at 1, 3, and 10 μg/kg). $n = 6$–8 rats/group in **B–E**. Results were analyzed using two-way ANOVA followed by Bonferroni's *post hoc* test and averaged data are presented as mean ± SD. $^{*}P < 0.05$, $^{**}P < 0.01$ *vs* Ctrl; $^{\#}P < 0.05$, $^{\#\#}P < 0.01$ *vs* HFD.

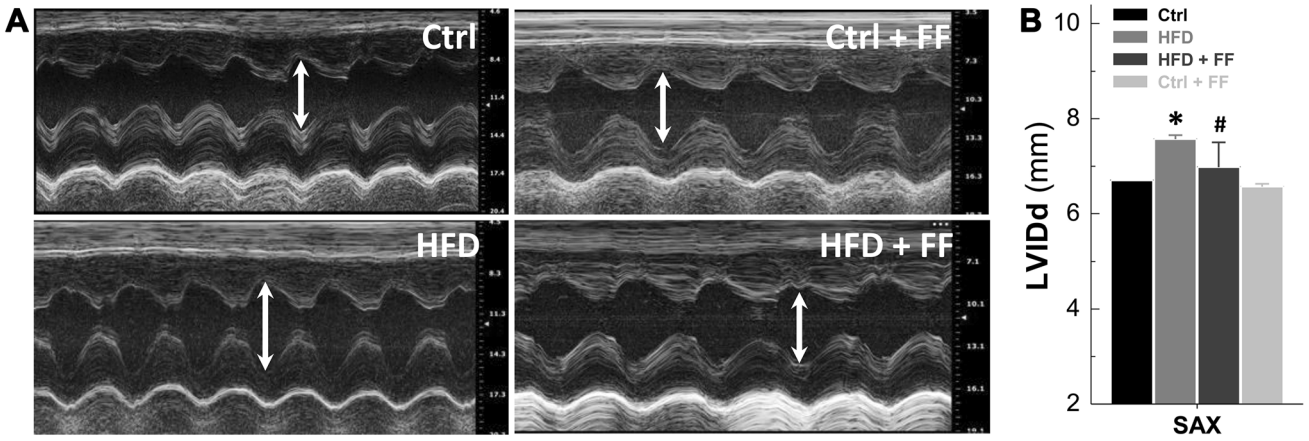

Fig. 3 Cardiac parameters in HFD and fenofibrate-treated rats. **A** Images representing the cardiac morphology of Ctrl, Ctrl + FF (4w), HFD, and HFD + FF (4w) rats in the SAX model. **B** Diastolic LVID (LVIDd, mm; n = 5/group). Results were analyzed using two-tailed unpaired Student's t-test and averaged data are presented as mean ± SD; $^{*}P < 0.05$ *vs* Ctrl, $^{\#}P < 0.05$ *vs* HFD.

Table 1 Ultrasound parameters of cardiac performance in control and fructose-fed hypertensive (HFD-HTN) rats before and after treatment with fenofibrate (FF).

Parameter	Ctrl	Ctrl + FF	HFD-HTN	HFD + FF
LVAWd	1.75 ± 0.08	1.80 ± 0.03	1.52 ± 0.16	1.71 ± 0.09
LVAWs	2.72 ± 0.09	2.77 ± 0.04	2.70 ± 0.16	3.35 ± 0.18
LVIDd	6.7 ± 0.3	6.57 ± 0.06	7.57 ± 0.08*	6.98 ± 0.52$^{\#}$
LVIDs	3.9 ± 0.4	3.93 ± 0.05	3.9 ± 0.4	3.9 ± 0.6
LVPWd	2.03 ± 0.09	2.32 ± 0.06	2.7 ± 0.5	2.07 ± 0.18
LVPWs	3.89 ± 0.16	3.89 ± 0.03	4.0 ± 0.3	4.1 ± 0.3
EF	70.59 ± 4.33	75.4 ± 0.53	73.07 ± 0.18	74.2 ± 8.2
FS	41.5 ± 3.6	46.8 ± 0.6	43.2 ± 0.4	47.6 ± 7.8

Ctrl, control rats; HFD, high fructose-drinking rats; FF, fenofibrate by gavage for 4 weeks. All data are presented as mean ± SD. $^{*}P < 0.05$ *vs* Ctrl; $^{\#}P < 0.05$ *vs* HFD. EF, ejection fraction; FS, fractional shortening; IVSs/IVSd, systolic/diastolic left ventricular septum thickness; LVIDs/LVIDd, systolic/diastolic left ventricular internal diameter; LVPWs/LVPWd, systolic/diastolic left ventricular posterior wall; SAX, short axis.

HFD rats ($P < 0.05$, n = 3 duplications for both; Fig. 4A). For protein expression, the results were consistent with the changes in mRNA, manifested as significant increases in both PPAR-α and PPAR-γ expression ($P < 0.05$, n = 4 and 5 duplications, respectively; Fig. 4B, C). Similar results were also found in the NTS and showed that the mRNA ($P < 0.01$, n = 5 duplications in both cases) and protein ($P < 0.05$, n = 5 duplications) expression of PPAR-α/γ were significantly upregulated (Fig. 4D–F). These findings strongly suggest that fenofibrate as the ligand binding with its receptor, a peroxisome proliferator-activated PPAR-α, would definitely modify the expression of downstream factors including mitochondrial uncoupling proteins (UCPs), lipoprotein lipase (LPL), and acyl-CoA oxidase (ACO) in the NG and NTS of hypertensive HFD rats.

Fenofibrate Upregulates Mitochondrial UCP2 Expression in the NTS and NG of HFD Rats

The UCPs have been demonstrated to be direct downstream factors for PPAR activation and the findings of significant up-regulation of PPARs in both the NG and NTS of HFD rats as well as the reversal action of fenofibrate provided reliable evidence leading us to explore the UCPs. We first screened the expression profiles of UCPs in the baroreflex afferent pathway along with LPL and ACO. Interestingly, the results showed that the mRNA expression of mitochondrial UCP2 (but not other UCPs) was dramatically higher in the NTS and NG, especially the latter, as well as LPL and ACO (Fig. 5), suggesting that UCP2 may be a crucial factor in baroreflex afferent

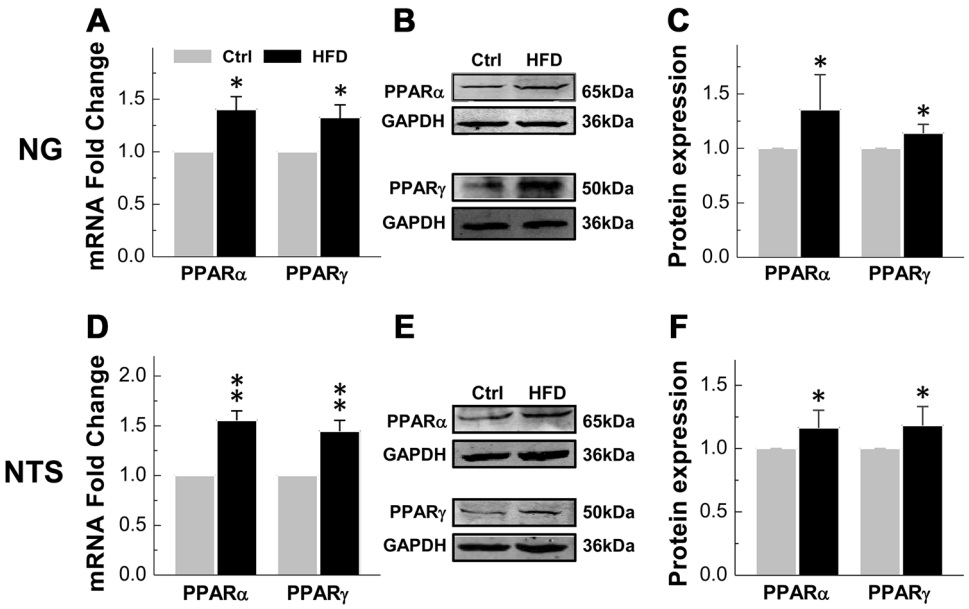

Fig. 4 Expression levels of PPAR-α/PPAR-γ in the NTS and NG of HFD rats. **A** PPAR-α/γ mRNA levels in the NG tissues of HFD and control rats ($n = 3$ duplications from 12 rats/group). **B**, **C** Protein levels of PPAR-α ($n = 4$ duplications from 16 rats/group) and PPAR-γ ($n = 5$ duplications from 20 rats/group) in the NG tissues of HFD and control rats. **D** PPAR-α/γ mRNA levels in the NTS tissues of HFD and control rats ($n = 5$ duplications from 15 rats/group). **E**, **F** PPAR-α and PPAR-γ protein expression in the NTS ($n = 5$ duplications from 15 rats/group). Results were analyzed using two-tailed unpaired Student's *t*-test, and averaged data are presented as mean ± SD. $^{*}P < 0.05$, $^{**}P < 0.01$ *vs* Ctrl. The gels were run under the same experimental conditions.

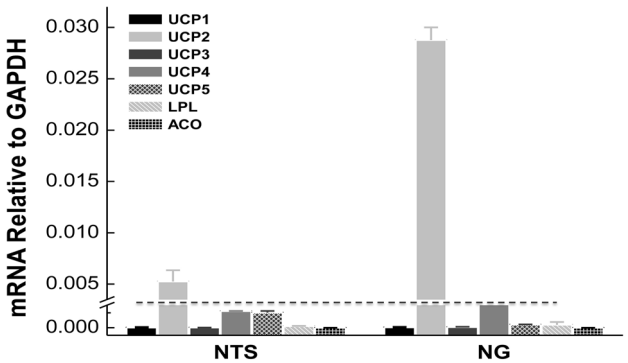

Fig. 5 Screening downstream factors of PPAR-α in HFD rats. The mRNA levels of downstream factors of PPAR-α, mitochondrial uncoupling proteins (UCPs), lipoprotein lipase (LPL), and acyl-CoA oxidase (ACO) in the NTS and NG tissues of HFD rats ($n = 3$ duplications). Results were analyzed using two-tailed unpaired Student's *t*-test, and averaged data are presented as mean ± SD.

function and the neural control of blood pressure. Based on our data showing upregulated PPAR-α/-γ in HFD-induced hypertensive rats, the UCP2 upregulation would be expected upon PPAR activation by PPAR activator fenofibrate. To investigate this, the HFD hypertensive rats were treated with fenofibrate and the protein expression of UCP2 was increased in the HFD + FF-4w group according to Western blot analyses ($P < 0.05$, $n = 5$ duplications each for NG and NTS; Fig. 6A–D). Meanwhile, superoxide, which represents the oxidative stress level, was significantly reduced by fenofibrate in HFD and normal control rats (Fig. 6F), consistent with the finding that superoxide dismutase activity increased in the NTS of HFD rats in the presence of fenofibrate (Fig. 6E). Thus, chronic fenofibrate treatment ameliorated not only UCPs but also oxidative stress in HFD rats.

Discussion

In this study, our novel results have demonstrated that chronic treatment with fenofibrate induces a clear anti-hypertensive effect in HFD hypertensive rats through mechanisms that ameliorate the function of baroreflex afferents by up-regulating mitochondrial UCP2 expression in the baroreflex afferent pathway after activation of PPAR-α/γ.

As we previously reported, HFD rats show significant hypertension with impaired BRS and an increased serum norepinephrine (NE) level [10], which is consistent with the current results. The pharmacological experiments revealed the beneficial effects of fenofibrate on blood pressure (SBP and MAP) and BRS in HFD rats during four weeks of chronic treatment with fenofibrate (Fig. 2). Furthermore, the markedly increased SBP (afterload) and LVIDd (preload) in HFD rats were both attenuated by fenofibrate. The reduction of SBP and LVIDd (Fig. 3, Table 1) by chronic fenofibrate treatment may be due at

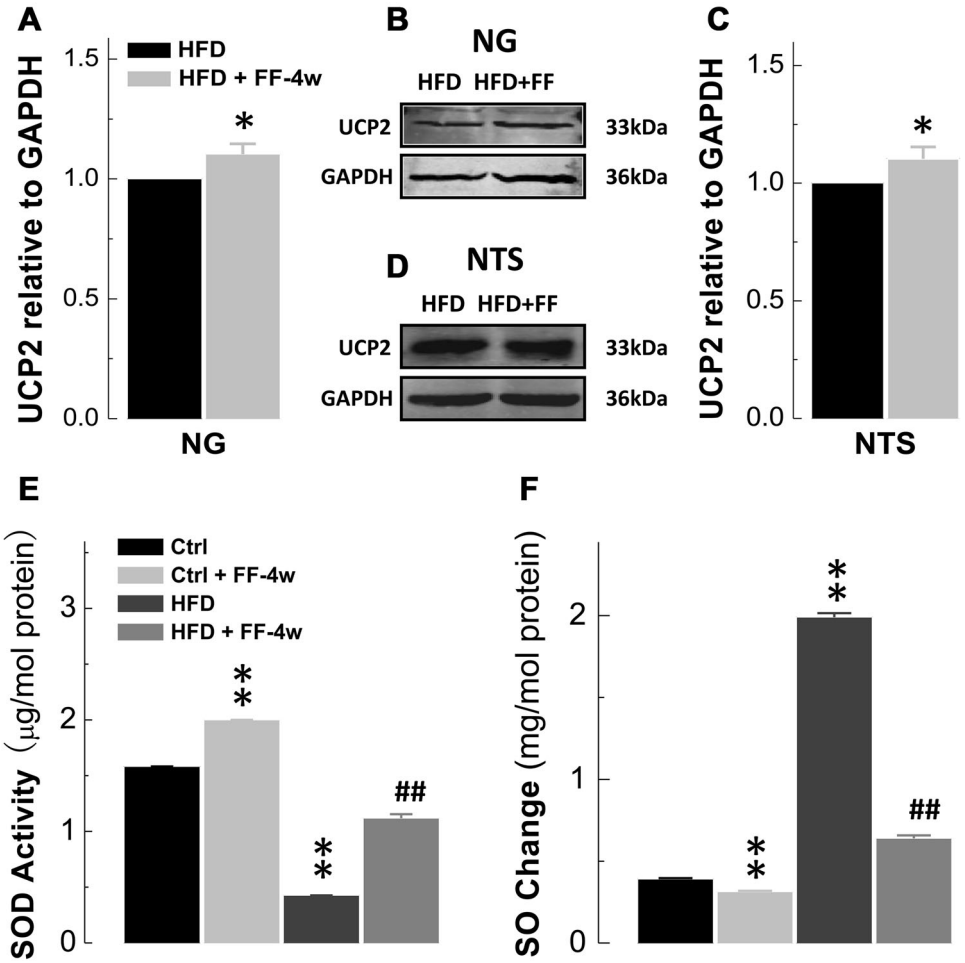

Fig. 6 Upregulation of UCP2 at the protein level in the NTS and NG of HFD rats after chronic fenofibrate treatment. **A**, **B** Protein expression of UCP2 in the NG tissues of HFD and HFD + FF-4w rats (n = 5 duplications from 10 rats/group). **C**, **D** Protein expression of UCP2 in the NTS tissues of HFD and HFD + FF-4w rats (n = 6 duplications from 24 rats/group). **E** Superoxide dismutase (SOD) levels in the NTS (n = 4/group). **F** Superoxide (SO) levels in the NTS (n = 4/group). Results were analyzed using two-tailed unpaired Student's t-test, and averaged data are presented as mean ± SD. $^{*}P < 0.05$ *vs* HFD, $^{**}P < 0.01$ *vs* Ctrl, $^{\#\#}P < 0.01$ *vs* HFD. The gels were run under the same experimental conditions.

least in part to its effects on sympathoinhibition (serum NE decreased) and BRS improvement. However, it is still controversial whether fenofibrate-induced PPARα activation has noxious effects on the development of ventricular dysfunction [38] and no improved effects on cardiac lipids in transgenic mice [39].

As far as we know, the direct targets and mechanisms underlying the neural control of blood pressure by fenofibrate have not been reported, and may involve its effects on the baroreflex and the sympathetic nervous system. The NTS is an important site of baroreflex integration, and we directly assessed the bradycardic (in response to PE) and tachycardic (in response to SNP) actions in response to an acutely applied pressor stimulus [40]. The BRS (ΔHR/ΔMAP) is a key marker along with heart rate variability representing the function and ability of the baroreflex to regulate blood pressure, and contributes to the alterations in heart rate and blood pressure [41]. Our data showed that fenofibrate did not alter BRS in HFD rats in the presence of SNP at increasing doses (Fig. 2E). A likely explanation for this is that it may be due to an inhibitory effect of fenofibrate on ventricular tachycardia [42] and partial resistance to the effect of SNP. Therefore, it is fundamental to investigate the roles of fenofibrate in the neural control of blood pressure to fully understand the protective effect. Apparently, fenofibrate ameliorated the hypertension and BRS impairment in HFD, strongly suggesting the involvement of the baroreflex afferent pathway in the antihypertensive action mediated by fenofibrate. This is supported by our recent finding [10] that FGF21 significantly reduces blood pressure in HFD rats with improved BRS.

Particularly, some of the downstream factors of PPARα/γ (UCPs, LPL, and ACO) participate in the regulation of metabolic syndrome and obesity [43–45]. We found that UCP2 was expressed more strongly than other UCPs in the NTS and NG (Fig. 5). UCP2 is a homologue of the UCP protein family of mitochondrial anion transporters that adapt to oxidative stress [46] by causing proton leakage across the mitochondrial inner membrane [47], using lipids as the fuel substrate [48]. Moreover, UCP2 is the only UCP that has been reported to be expressed in the brain [47], and promotes an important antihypertensive effect *via* the transcriptional up-regulation of mitochondrial UCP2 against oxidative stress in spontaneously hypertensive rats

[23]. Our data fully support our hypothesis of PPAR-α/PPAR-γ upregulation in the NG and NTS regions in HFD rats (Fig. 4). Meanwhile, the functional upregulation of UCP2 in the NTS and NG by chronic fenofibrate treatment resulted in oxidative stress improvement (Fig. 6). Fenofibrate activated the PPAR-α/UCP2 pathway to control blood pressure *via* the baroreflex afferent pathway. Thus, it is attractive to investigate the role of fenofibrate in hypertension by the knockdown/knockout of receptors (PPAR-α/UCP2) in the NTS or NG in HFD rats in further investigations. This would complete the mechanism underlying how chronic treatment with fenofibrate has a significant antihypertensive effect by upregulation of UCP2 through the baroreflex afferent pathway after PPAR-α activation in HFD rats. Furthermore, our immunohistochemistry showed that PPAR-α/PPAR-γ are extensively distributed in the brainstem, but further evidence is needed to further determine whether fenofibrate acts on other autonomic areas in the central nervous system.

In brief, the findings of this investigation confirmed that, through PPAR-α activation, fenofibrate has a significant antihypertensive effect by up-regulation of mitochondrial UCP2, and amelioration of the oxidative stress level *via* novel targets (NTS and NG) within the baroreflex afferent pathway (Fig. 7).

Perspectives

Because of the pivotal role of the baroreflex afferent pathway in the neural control of hypertension, our investigation of PPAR-α activation and upregulation of the mitochondrial anti-oxidant UCP2 through the baroreflex afferent pathway underpins the significant anti-hypertensive action of chronic fenofibrate treatment. Therefore, it opens a new view for novel therapeutic strategies against hypertension.

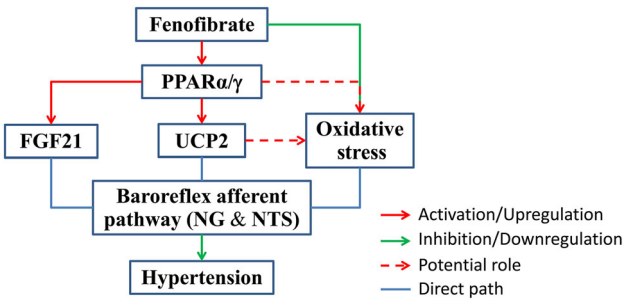

Fig. 7 Schematic of the working hypothesis. Interaction of PPARα/γ with fibroblast growth factor 21 (FGF21) was shown to regulate the blood pressure of HFD rats by modulating baroreflex afferent function in a previous study [10]. In the current working model, fenofibrate (as a PPAR-α agonist) up-regulates PPAR-α and PPAR-γ (synergistically with PPAR-α) and directly contributes to the up-regulation of UCP2 and improvement of oxidative stress *via* the baroreflex afferent pathway in the HFD model.

Acknowledgements This work was supported by the National Natural Science Foundation of China (81573431 and 81773731).

Compliance with Ethical Standards

Conflict of interest These authors declare no conflict of interest.

References

1. Kersten S, Desvergne B, Wahli W. Roles of PPARs in health and disease. Nature 2000, 405: 421–424.
2. Lu KL, Xu WN, Li XF, Liu WB, Wang LN, Zhang CN. Hepatic triacylglycerol secretion, lipid transport and tissue lipid uptake in blunt snout bream (*Megalobrama amblycephala*) fed high-fat diet. Aquaculture 2013, 408–409: 160–168.
3. Vikramadithyan RK, Hirata K, Yagyu H, Hu Y, Augustus A, Homma S, *et al.* Peroxisome proliferator-activated receptor agonists modulate heart function in transgenic mice with lipotoxic cardiomyopathy. J Pharmacol Exp Ther 2005, 313: 586–593.
4. Rani N, Bharti S, Bhatia J, Nag TC, Ray R, Arya DS. Chrysin, a PPAR-γ agonist improves myocardial injury in diabetic rats through inhibiting AGE-RAGE mediated oxidative stress and inflammation. Chem Biol Interact 2016, 250: 59–67.
5. Sun K, Park J, Kim M, Scherer PE. Endotrophin, a multifaceted player in metabolic dysregulation and cancer progression, is a predictive biomarker for the response to PPARgamma agonist treatment. Diabetologia 2017, 60: 24–29.
6. Davidson MH, Rosenson RS, Maki KC, Nicholls SJ, Ballantyne CM, Mazzone T, *et al.* Effects of fenofibric acid on carotid intima-media thickness in patients with mixed dyslipidemia on atorvastatin therapy: randomized, placebo-controlled study (FIRST). Arterioscler Thromb Vasc Biol 2014, 34: 1298–1306.
7. Petrescu AD, Mcintosh AL, Storey SM, Huang H, Martin GG, Landrock D, *et al.* High glucose potentiates L-FABP mediated fibrate induction of PPARα in mouse hepatocytes. Biochim Biophys Acta 2013, 1831: 1412–1425.
8. Zhao X, Li LY. PPAR-alpha agonist fenofibrate induces renal CYP enzymes and reduces blood pressure and glomerular hypertrophy in Zucker diabetic fatty rats. Am J Nephrol 2008, 28: 598–606.
9. Yuan X, Tsujimoto K, Hashimoto K, Kawahori K, Hanzawa N, Hamaguchi M, *et al.* Epigenetic modulation of Fgf21 in the perinatal mouse liver ameliorates diet-induced obesity in adulthood. Nat Commun 2018, 9: 636.
10. He JL, Zhao M, Xia JJ, Guan J, Liu Y, Wang LQ, *et al.* FGF21 ameliorates the neurocontrol of blood pressure in the high fructose-drinking rats. Sci Rep 2016, 6: 29582.
11. Li L, Emmett N, Mann D, Zhao X. Fenofibrate attenuates tubulointerstitial fibrosis and inflammation through suppression of nuclear factor-κB and transforming growth factor-β1/Smad3 in diabetic nephropathy. Exp Biol Med 2010, 235: 383–391.
12. Davis TM, Ting R, Best JD, Donoghoe MW, Drury PL, Sullivan DR, *et al.* Effects of fenofibrate on renal function in patients with type 2 diabetes mellitus: the Fenofibrate Intervention and Event Lowering in Diabetes (FIELD) Study. Diabetologia 2011, 54: 280–290.

13. Jia Z, Rui X, Liu G, Ling L, Yang J, Pi G, *et al.* HMGB1 is involved in the protective effect of the PPARα agonist fenofibrate against cardiac hypertrophy. PPAR Res 2014, 2014: 541394.
14. Barbiero JK, Santiago RM, Persike DS, Da SFM, Tonin FS, Da CC, *et al.* Neuroprotective effects of peroxisome proliferator-activated receptor alpha and gamma agonists in model of parkinsonism induced by intranigral 1-methyl-4-phenyl-1,2,3,6-tetrahyropyridine. Behav Brain Res 2014, 274: 390–399.
15. Ibarra-Lara L, Cervantes-Pérez LG, Pérez-Severiano F, Valle LD, Rubio-Ruíz E, Soria-Castro E, *et al.* PPARα stimulation exerts a blood pressure lowering effect through different mechanisms in a time-dependent manner. Eur J Pharmacol 2010, 627: 185–193.
16. Tordjman KM, Semenkovich CF, Coleman T, Yudovich R, Bak S, Osher E, *et al.* Absence of peroxisome proliferator-activated receptor-alpha abolishes hypertension and attenuates atherosclerosis in the Tsukuba hypertensive mouse. Hypertension 2007, 50: 945–951.
17. Ueno H, Saitoh Y, Mizuta M, Shiiya T, Noma K, Mashiba S, *et al.* Fenofibrate ameliorates insulin resistance, hypertension and novel oxidative stress markers in patients with metabolic syndrome. Obes Res Clin Pract 2011, 5: e267–360.
18. Liu Y, Zhou JY, Zhou YH, Wu D, He JL, Han LM, *et al.* Unique expression of angiotensin type-2 receptor in sex-specific distribution of myelinated Ah-type baroreceptor neuron contributing to sex-dimorphic neurocontrol of circulation. Hypertension 2016, 67: 783–791.
19. Salman IM, Hildreth CM, Ameer OZ, Phillips JK. Differential contribution of afferent and central pathways to the development of baroreflex dysfunction in chronic kidney disease. Hypertension 2014, 63: 804–810.
20. Huber DA, Schreihofer AM. Attenuated baroreflex control of sympathetic nerve activity in obese Zucker rats by central mechanisms. J Physiol 2010, 588: 1515–1525.
21. Kaneko K, Yamada T, Tsukita S, Takahashi K, Ishigaki Y, Oka Y, *et al.* Obesity alters circadian expressions of molecular clock genes in the brainstem. Brain Res 2009, 1263: 58–68.
22. Borges GR, Morgan DA, Ketsawatsomkron P, Mickle AD, Thompson AP, Cassell MD, *et al.* Interference with peroxisome proliferator-activated receptor-gamma in vascular smooth muscle causes baroreflex impairment and autonomic dysfunction. Hypertension 2014, 64: 590–596.
23. Chan SH, Wu KL, Kung PS, Chan JY. Oral intake of rosiglitazone promotes a central antihypertensive effect via upregulation of peroxisome proliferator-activated receptor-gamma and alleviation of oxidative stress in rostral ventrolateral medulla of spontaneously hypertensive rats. Hypertension 2010, 55: 1444–1453.
24. Braga VA, Colombari E, Jovita MG. Angiotensin II-derived reactive oxygen species underpinning the processing of the cardiovascular reflexes in the medulla oblongata. Neurosci Bull 2011, 27: 269–274.
25. Zhou FM, Cheng RX, Wang S, Huang Y, Gao YJ, Zhou Y, *et al.* Antioxidants attenuate acute and chronic itch: peripheral and central mechanisms of oxidative stress in pruritus. Neurosci Bull 2017, 33: 1–13.
26. Souza BM, Assmann TS, Kliemann LM, Gross JL, Canani LH, Crispim D. The role of uncoupling protein 2 (UCP2) on the development of type 2 diabetes mellitus and its chronic complications. Arq Bras Endocrinol Metabol 2011, 55: 239–248.
27. Lu M, Zhao FF, Tang JJ, Su CJ, Fan Y, Ding JH, *et al.* The neuroprotection of hydrogen sulfide against MPTP-induced dopaminergic neuron degeneration involves uncoupling protein 2 rather than ATP-sensitive potassium channels. Antioxid Redox Signal 2012, 17: 849–859.
28. Guimaraes PS, Oliveira MF, Braga JF, Nadu AP, Schreihofer A, Santos RA, *et al.* Increasing angiotensin-(1-7) levels in the brain attenuates metabolic syndrome-related risks in fructose-fed rats. Hypertension 2014, 63: 1078–1085.
29. Tran LT, Yuen VG, Mcneill JH. The fructose-fed rat: a review on the mechanisms of fructose-induced insulin resistance and hypertension. Mol Cell Biochem 2009, 332: 145–159.
30. Yu Y, Xue BJ, Wei SG, Zhang ZH, Beltz TG, Guo F, *et al.* Activation of central PPAR-gamma attenuates angiotensin II-induced hypertension. Hypertension 2015, 66: 403–411.
31. Pierzchala M, Fakhfakh M. Cardioprotective Effect of Combination of Enalapril and Fenofibrate. Lap Lambert Academic Publishing, 2011: 2394–2397.
32. Singh G, Khan MU, Khanam R. Protective role of fibrates in cardiac ischemia/reperfusion. J Adv Pharm Technol Res 2012, 3: 188–192.
33. Arnold AC, Shaltout HA, Gallagher PE, Diz DI. Leptin impairs cardiovagal baroreflex function at the level of the solitary tract nucleus. Hypertension 2009, 54: 1001–1008.
34. Zhang D, Liu J, Tu H, Muelleman RL, Cornish KG, Li YL. In-vivo transfection of manganese superoxide dismutase gene or NFκB shRNA in nodose ganglia improves aortic baroreceptor function in heart failure rats. Hypertension 2014, 63: 88.
35. Qiao GF, Li BY, Lu YJ, Fu YL, Schild JH. 17Beta-estradiol restores excitability of a sexually dimorphic subset of myelinated vagal afferents in ovariectomized rats. Am J Physiol Cell Physiol 2009, 297: C654–C664.
36. Schmittgen TD, Livak KJ. Analyzing real-time PCR data by the comparative C(T) method. Nat Protoc 2008, 3: 1101.
37. Li JN, Li XL, He J, Wang JX, Zhao M, Liang XB, *et al.* Sex- and afferent-specific differences in histamine receptor expression in vagal afferents of rats: A potential mechanism for sexual dimorphism in prevalence and severity of asthma. Neuroscience 2015, 303: 166–177.
38. Kaimoto S, Hoshino A, Ariyoshi M, Okawa Y, Tateishi S, Ono K, *et al.* Activation of PPARα in the early stage of heart failure maintained myocardial function and energetics in pressure overload heart failure. Am J Physiol Heart Circ Physiol 2016, 312: H305–H313.
39. Duncan JG, Bharadwaj KG, Fong JL, Mitra R, Sambandam N, Courtois MR, *et al.* Rescue of cardiomyopathy in PPARα transgenic mice by deletion of lipoprotein lipase identifies sources of cardiac lipids and PPARα activators. Circulation 2010, 121: 426–435.
40. Evans LC, Ivy JR, Caitlin W, Mcnairn JA, Menzies RI, Christensen TH, *et al.* Conditional deletion of Hsd11b2in the brain causes salt appetite and hypertension. Circulation 2016, 133: 1360–1370.
41. Linz D, Mahfoud F, Schotten U, Ukena C, Neuberger HR, Wirth K, *et al.* Effects of electrical stimulation of carotid baroreflex and renal denervation on atrial electrophysiology. J Cardiovasc Electrophysiol 2013, 24: 1028–1033.
42. Bukhari IA, Almotrefi AA, Mohamed OY, Masri AAA. Fenofibrate inhibits ischemia-reperfusion induced cardiac arrhythmias in isolated rat hearts. FASEB J 2013, 27: 652.
43. Ruby MA, Goldenson B, Orasanu G, Johnston TP, Plutzky J, Krauss RM. VLDL hydrolysis by LPL activates PPAR-alpha through generation of unbound fatty acids. J Lipid Res 2010, 51: 2275–2281.
44. Harms M, Seale P. Brown and beige fat: development, function and therapeutic potential. Nat Med 2013, 19: 1252–1263.
45. Nam JS, Chung HJ, Jang MK, Jung IA, Park SH, Cho SI, *et al.* Sasa borealis extract exerts an antidiabetic effect via activation of the AMP-activated protein kinase. Nutr Res Pract 2013, 7: 15–21.
46. Pons DG, Nadal-Serrano M, Torrens-Mas M, Valle A, Oliver J, Roca P. UCP2 inhibition sensitizes breast cancer cells to therapeutic agents by increasing oxidative stress. Free Radic Biol Med 2015, 86: 67–77.
47. Cardoso S, Santos MS, Moreno A, Moreira PI. UCP2 and ANT differently modulate proton-leak in brain mitochondria of long-term hyperglycemic and recurrent hypoglycemic rats. J Bioenerg Biomembr 2013, 45: 397–407.
48. Diano S, Horvath TL. Mitochondrial uncoupling protein 2 (UCP2) in glucose and lipid metabolism. Trends Mol Med 2012, 18: 52–58.